

Spin dynamics of a $J_1 - J_2$ antiferromagnet and its implications for iron pnictides

Pallab Goswami,¹ Rong Yu,¹ Qimiao Si,¹ and Elihu Abrahams²

¹*Department of Physics and Astronomy, Rice University, Houston, Texas 77005, USA*

²*Department of Physics and Astronomy, University of California, Los Angeles, California 90095, USA*

(Received 6 October 2010; revised manuscript received 30 August 2011; published 12 October 2011)

Motivated by the recent observation of antiferromagnetic correlations in the paramagnetic phase of iron pnictides, we study the finite-temperature spin dynamics of a two-dimensional $J_1 - J_2$ antiferromagnet. We consider the paramagnetic phase in the regime of a $(\pi, 0)$ collinear ground state, using the modified spin wave theory. Below the mean-field Ising transition temperature, we identify short-range anisotropic antiferromagnetic correlations. We show that the dynamical structure factor $\mathcal{S}(\mathbf{q}, \omega)$ contains elliptic features in the momentum space, and determine its variation with temperature and energy. Implications for the spin-dynamical experiments in the iron pnictides are discussed.

DOI: [10.1103/PhysRevB.84.155108](https://doi.org/10.1103/PhysRevB.84.155108)

PACS number(s): 75.10.Jm, 74.70.Xa, 75.40.Gb

I. INTRODUCTION

High-temperature superconductivity in the iron pnictides^{1,2} arises by doping antiferromagnetic parent compounds.³ Hence, the strength of the electronic correlations, the nature of magnetism, and the relationship between magnetic excitations and the superconductivity are important issues for understanding the emergence of high-temperature superconductivity in these materials. In the parent iron pnictides, the Néel transition into a $(\pi, 0)$ antiferromagnet is either preceded by or concomitant with a tetragonal-to-orthorhombic structural transition. The $(\pi, 0)$ magnetic order by itself can be understood either by invoking a local moment $J_1 - J_2$ model⁴⁻¹¹ or an itinerant model with nearly nested electron and hole pockets.¹²⁻¹⁴

The experimentally observed “bad metal” behavior, the Drude-weight suppression,^{15,16} and the temperature-induced spectral-weight transfer¹⁶⁻¹⁸ place these materials near to a Mott transition,^{4,9,19,20} a Mott insulator can emerge when the iron square lattice either expands²¹ or contains ordered vacancies.²² In a metallic system close to a Mott transition, quasilocal moments are expected to arise; this picture is further supported by the experimental observation of zone boundary spin wave excitations in the magnetically ordered state at low temperatures.²³ The inelastic neutron scattering experiments demonstrated the need for an anisotropic $J_1 - J_2$ model with $J_{1x} \neq J_{1y}$, which may reflect an orbital ordering²⁴⁻²⁶ while pointing to the relevance of magnetic frustration from the extracted ratio $(J_{1x} + J_{1y})/2J_2 \sim 1$.²³ Therefore, results in the tetragonal, paramagnetic phase of the parent compounds are of great importance for understanding the relevance of an isotropic $J_1 - J_2$ model as well as the strength of the underlying magnetic frustration. Recent inelastic neutron scattering measurements of Diallo *et al.*²⁷ on the tetragonal, paramagnetic phase of CaFe_2As_2 represent a first step in this direction. Even above the concomitant first-order structural and Néel transition temperature, they have observed anisotropic spin dynamics around the $(\pi, 0)$ wave vector, and the inferred ratio $J_1/J_2 \sim 0.55$ is similar to that of the ordered phase.

Motivated by these experimental results we study the spin dynamics of a two-dimensional $J_1 - J_2$ antiferromagnet. While theoretical studies exist on the order-from-disorder phenomenon and phase diagram of the $J_1 - J_2$ model,^{28,29} the spin dynamics in the paramagnetic phase of the model

in the $(\pi, 0)$ collinear regime has not yet been systematically studied. We carry out the calculations using a modified spin wave theory,³⁰ which incorporates the $1/S$ corrections that are important for capturing the order-from-disorder phenomenon and the associated dynamical properties. We discuss the implications of our results for the iron pnictides, including the role of itinerant electrons.

Our paper is organized as follows. In Sec. II we introduce the relevant $J_1 - J_2$ model and describe the modified spin wave theory calculations. In Sec. III we analyze the excitation spectrum obtained from the modified spin wave theory, and associated behavior of the spin-spin correlation length. In Sec. IV we analyze the dynamic structure factor calculated by using the modified spin wave theory results. In Sec. V we consider the fluctuation effects due to itinerant electrons within a Ginzburg-Landau framework. In Sec. VI we describe the relation between our theoretical results and the experimental data obtained in the paramagnetic phase of iron pnictides. We provide a summary of our work in Sec. VII. The technical details of fitting the experimental data and consideration of interplanar exchange coupling using modified spin wave theory are respectively relegated to Appendix A and Appendix B.

II. MODEL AND MODIFIED SPIN WAVE THEORY

The model is defined by the Hamiltonian

$$H = J_1 \sum_{\langle ij \rangle} \mathbf{S}_i \cdot \mathbf{S}_j + J_2 \sum_{\langle\langle ij \rangle\rangle} \mathbf{S}_i \cdot \mathbf{S}_j, \quad (1)$$

where J_1 and J_2 respectively denote the antiferromagnetic exchange couplings between spins located in the nearest ($\langle ij \rangle$) and next-nearest neighbor ($\langle\langle ij \rangle\rangle$) sites on a square lattice. Classically, for $J_2/J_1 > \alpha_c = 0.5$, the lattice decouples into two independently Néel ordered, interpenetrating lattices, and the angle ϕ between the staggered magnetizations of these two sublattices, as illustrated in the Fig. 1 inset, is arbitrary. An order-from-disorder transition at temperature T_σ breaks the fourfold rotational symmetry of the square lattice down to a twofold rotational symmetry of the rectangular lattice, and $\phi = 0, \pi$ emerge as degenerate ground states at $T = 0$.²⁸ Since quantum fluctuations make $\alpha_c > 0.5$, for definiteness we will focus on $J_2/J_1 > 1$.

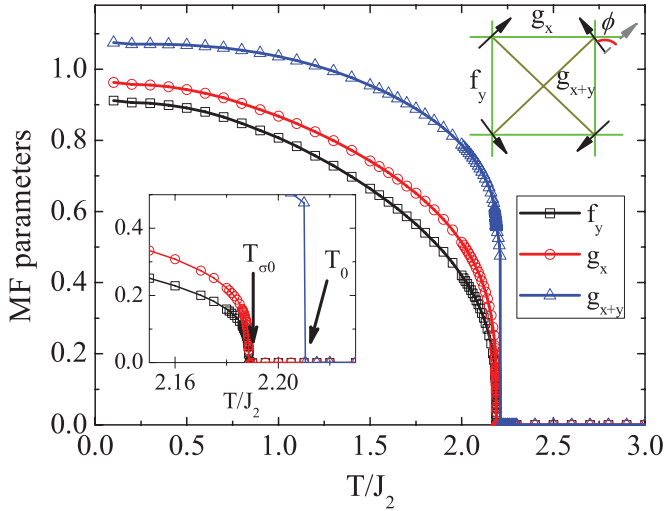


FIG. 1. (Color online) The temperature dependence of the mean-field parameters, for $S = 1$ and $J_1/J_2 = 0.8$. The decoupled Néel sublattices are illustrated in the upper right corner, which also defines the angle ϕ .

We define a local spin quantization axis along the classical ordering direction at each site (Ω_i^{cl}), as illustrated in an inset to Fig. 1. We then introduce the corresponding Dyson-Maleev (DM) boson representation for the spin operators at each site: $\mathbf{S}_i \cdot \Omega_i^{cl} = S - a_i^\dagger a_i$, as well as $\mathbf{S}_i^+ = \sqrt{2S}(1 - a_i^\dagger a_i/2S)a_i$ and $\mathbf{S}_i^- = \sqrt{2S}a_i^\dagger$. The modified spin wave theory³⁰ treats the self-energy of the a bosons as a static quantity, which renormalizes their dispersion; in this respect, it is similar to the large- N Schwinger boson mean-field theory.³¹ Following Takahashi,^{30,32} we express the Hamiltonian, Eq. (1), in terms

of the DM bosons in momentum space. The procedure is to minimize the free energy $\mathcal{F} = \langle H \rangle - TS$ under the constraint of zero magnetization, $\langle S - a_i^\dagger a_i \rangle = 0$, with respect to variational parameters which enter \mathcal{F} . These are the boson dispersion $\epsilon_{\mathbf{k}}$, the angle ϕ , and the Bogoliubov angle $\theta_{\mathbf{k}}$. The latter enters in a Bogoliubov transformation that mixes the operators of the two interpenetrating Néel sublattices and renders the nonzero temperature density matrix diagonal.³⁰ The equal time correlators $\langle \mathbf{S}_i \cdot \mathbf{S}_j \rangle$ can be written in terms of expectation values like $\langle a_i^\dagger a_j \rangle$. Therefore, we define ferromagnetic and antiferromagnetic bond correlations $f_{ij} = \langle a_i^\dagger a_j \rangle = \langle a_i a_j^\dagger \rangle$ and $g_{ij} = \langle a_i a_j \rangle = \langle a_i^\dagger a_j^\dagger \rangle$. The explicit expressions for the bond correlations are given by

$$f_{ij} = \frac{1}{N} \sum_{\mathbf{k}} \cosh 2\theta_{\mathbf{k}} \left(n_{\mathbf{k}} + \frac{1}{2} \right) \exp(-i\mathbf{k} \cdot \mathbf{r}_{ij}), \quad (2)$$

$$g_{ij} = \frac{1}{N} \sum_{\mathbf{k}} \sinh 2\theta_{\mathbf{k}} \left(n_{\mathbf{k}} + \frac{1}{2} \right) \exp(-i\mathbf{k} \cdot \mathbf{r}_{ij}), \quad (3)$$

where $n_{\mathbf{k}} = [\exp(\epsilon_{\mathbf{k}}/T) - 1]^{-1}$ is the Bose occupation factor.

In terms of f_{ij} and g_{ij} the equal time spin correlator $\langle \mathbf{S}_i \cdot \mathbf{S}_j \rangle$ can be expressed as

$$\langle \mathbf{S}_i \cdot \mathbf{S}_j \rangle = \cos^2 \frac{\phi_{ij}}{2} \left[S + \frac{1}{2} - f(0) + f_{ij} \right]^2 - \sin^2 \frac{\phi_{ij}}{2} \left[S + \frac{1}{2} - f(0) + g_{ij} \right]^2, \quad (4)$$

where $\phi_{ij} = \phi, \pi - \phi, \pi$, for horizontal, vertical, and diagonal bonds, respectively (see Fig. 1). Using the expression for $\langle \mathbf{S}_i \cdot \mathbf{S}_j \rangle$ for different bonds, the total energy can be written as

$$E = \frac{J_1 N}{2} \sum_{\delta_1 = \pm \hat{x}} \left[\cos^2 \frac{\phi}{2} \left(S + \frac{1}{2} - f(0) + f_x \right)^2 - \sin^2 \frac{\phi}{2} \left(S + \frac{1}{2} - f(0) + g_x \right)^2 \right] + \frac{J_1 N}{2} \sum_{\delta_2 = \pm \hat{y}} \left[\sin^2 \frac{\phi}{2} \left(S + \frac{1}{2} - f(0) + f_y \right)^2 - \cos^2 \frac{\phi}{2} \left(S + \frac{1}{2} - f(0) + g_y \right)^2 \right] - \frac{J_2 N}{2} \sum_{\delta_3 = \pm \hat{x} \pm \hat{y}} \left(S + \frac{1}{2} - f(0) + g_{x+y} \right)^2. \quad (5)$$

Notice that the expression for total energy only contains the nearest and next-nearest neighbor bond correlation parameters f_x, f_y, g_x, g_y , and g_{x+y} . The constraint of zero magnetization, appropriate for $T > T_N$ (for the two-dimensional problem $T_N = 0$), is enforced by the Lagrange multiplier μ . Minimizing $E - TS - \mu f(0)$ with respect to $\epsilon_{\mathbf{k}}, \phi, \theta_{\mathbf{k}}$, we obtain $\tanh 2\theta_{\mathbf{k}} = A_{\mathbf{k}}/B_{\mathbf{k}}, \epsilon_{\mathbf{k}} = \sqrt{B_{\mathbf{k}}^2 - A_{\mathbf{k}}^2}$ and $\sin \phi (f_y^2 + g_y^2 - f_x^2 - g_x^2) = 0$, where

$$A_{\mathbf{k}} = 2J_1 \left(\sin^2 \frac{\phi}{2} g_x C_{x,\mathbf{k}} + \cos^2 \frac{\phi}{2} g_y C_{y,\mathbf{k}} \right) + 4J_2 g_{x+y} C_{x+y,\mathbf{k}}, \quad (6)$$

$$B_{\mathbf{k}} = 2J_1 \left(\sin^2 \frac{\phi}{2} (g_x - f_y) + \cos^2 \frac{\phi}{2} (g_y - f_x) \right) + 2J_1 \left(\cos^2 \frac{\phi}{2} f_x C_{x,\mathbf{k}} + \sin^2 \frac{\phi}{2} f_y C_{y,\mathbf{k}} \right) + 4J_2 g_{x+y} - \mu, \quad (7)$$

and we have introduced the form factors $C_{x,\mathbf{k}} = \cos k_x a, C_{y,\mathbf{k}} = \cos k_y a$, and $C_{x+y,\mathbf{k}} = \cos k_x a \cos k_y a$. Now using $\tanh 2\theta_{\mathbf{k}} = A_{\mathbf{k}}/B_{\mathbf{k}}$ in Eq. (3), we obtain the following set of self-consistent

equations:

$$f_\alpha = \frac{1}{N} \sum_{\mathbf{k}} \frac{B_{\mathbf{k}}}{\epsilon_{\mathbf{k}}} \left(n_{\mathbf{k}} + \frac{1}{2} \right) C_{\alpha, \mathbf{k}}, \quad \alpha = x, y, \quad (8)$$

$$g_\alpha = \frac{1}{N} \sum_{\mathbf{k}} \frac{A_{\mathbf{k}}}{\epsilon_{\mathbf{k}}} \left(n_{\mathbf{k}} + \frac{1}{2} \right) C_{\alpha, \mathbf{k}}, \quad \alpha = x, y, x+y, \quad (9)$$

$$S + \frac{1}{2} = f(0) = \frac{1}{N} \sum_{\mathbf{k}} \frac{B_{\mathbf{k}}}{\epsilon_{\mathbf{k}}} \left(n_{\mathbf{k}} + \frac{1}{2} \right). \quad (10)$$

We identify two important temperature scales T_0 and $T_{\sigma 0}$ such that $T_0 > T_{\sigma 0}$, by solving the self-consistent equations. The temperature $T_0 = J_2(S + 1/2)[\log(1/S + 1)]^{-1}$ marks the onset of the largest bond correlation g_{x+y} , while $T_{\sigma 0}$ marks the onset of nearest-neighbor bond correlations. For $T > T_0$, all the bond correlations vanish and we have decoupled local moment behavior. The first-order transition from the correlated to decoupled moment state at T_0 is an artifact of the mean-field theory.³⁰ In the temperature range $T_{\sigma 0} < T < T_0$, the sublattice angle ϕ remains arbitrary, and the system has C_{4v} rotational symmetry. For $T < T_{\sigma 0}$ there are two degenerate solutions $\phi = \pi$, with $g_y = f_x = 0, g_x \neq 0, f_y \neq 0, g_x \neq f_y$, and $\phi = 0$, with $x \leftrightarrow y$ switching. An Ising order parameter, which is defined classically as $\sigma = \mathbf{\Omega}_1 \cdot \mathbf{\Omega}_2 = \cos \phi$, is modified to $\sigma \propto 2(\cos^2 \frac{\phi}{2}(f_x^2 + g_y^2) - \sin^2 \frac{\phi}{2}(f_y^2 + g_x^2))$, and becomes nonzero below $T_{\sigma 0}$. We identify this temperature as the mean-field ‘‘Ising transition’’ temperature; fluctuations will reduce the actual transition to $T_\sigma < T_{\sigma 0}$. In the following, we will focus on the state with $\phi = \pi$. The spectrum is gapped at any nonzero temperature, but becomes gapless at $T = 0$ giving rise to $(\pi, 0)$ antiferromagnetic order via a Bose condensation.

III. LOW-ENERGY SPECTRUM AND CORRELATION LENGTH

The boson dispersion $\epsilon_{\mathbf{k}}$ is shown in Fig. 2. For $\phi = \pi$ and $T \ll T_{\sigma 0}$, the low-energy physics is governed by the excitations in the vicinity of the ordering vector $(\pi, 0)$, where the absolute minimum of the dispersion is located. Near $(\pi, 0)$, the dispersion can be approximated by

$$\epsilon_{\mathbf{k}} = [v_{1x}^2(\pi - k_x)^2 + v_{1y}^2 k_y^2 + \Delta_1^2]^{1/2}, \quad (11)$$

$$\Delta_1 = [-\mu(8J_2g_{x+y} + 4J_1g_x - \mu)]^{1/2}, \quad (12)$$

$$v_{1x} = a(4J_2g_{x+y} + 2J_1g_x), \quad (13)$$

$$v_{1y} = a[(4J_2g_{x+y} + 2J_1g_x)(4J_2g_{x+y} - 2J_1f_y) + 2J_1f_y\mu]^{1/2}. \quad (14)$$

Similarly in the vicinity of $(0, \pi)$, the excitation can be approximated as

$$\epsilon_{\mathbf{k}} = [v_{2x}^2 k_x^2 + v_{2y}^2(\pi - k_y)^2 + \Delta_2^2]^{1/2}, \quad (15)$$

$$\Delta_2 = [(8J_2g_{x+y} - 4J_1f_y - \mu)(4J_1g_x - 4f_y - \mu)]^{1/2}, \quad (16)$$

$$v_{2x} = a(4J_2g_{x+y} - 2J_1g_x), \quad (17)$$

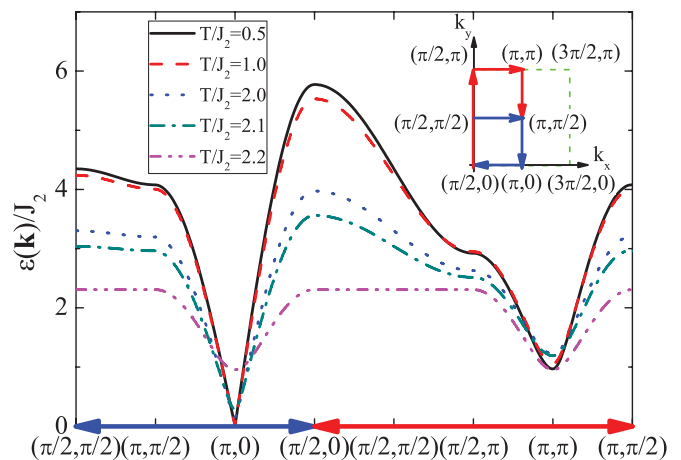


FIG. 2. (Color online) The dispersion $\epsilon_{\mathbf{k}}$ along high symmetry directions in the paramagnetic Brillouin zone for different temperatures and $S = 1$, $J_1/J_2 = 0.8$. The curves from top to bottom viewed at the left end are for $T/J_2 = 0.5, 1.0, 2.0, 2.1, 2.2$. The plotted directions in the Brillouin zone are displayed in the upper right corner.

$$v_{2y} = a[4J_2g_{x+y}(4J_2g_{x+y} - 2J_1g_x) + 2J_1f_y(4J_2g_{x+y} + 2J_1g_x - 4J_1f_y - \mu)]^{1/2}. \quad (18)$$

At low temperatures $T \ll T_{\sigma 0}$, the Lagrange multiplier μ is exponentially small, and $\Delta_1 \ll \Delta_2$. Therefore the spin-spin correlation length at low temperatures will be dominated by the smallest gap $\Delta_1 = T \exp[-\Delta_J/T]$, where $\Delta_J = 2\pi\rho$ is the Josephson energy, with $\rho = m_0v_{1y}$ being the stiffness and m_0 the staggered magnetization at $T = 0$. The velocity anisotropy yields two correlation lengths, $\xi_x = v_{1x}/\Delta_1$ and $\xi_y = v_{1y}/\Delta_1$.

The low-energy excitations around $(\pi, 0)$ can also be described in terms of an anisotropic $O(3)$ nonlinear sigma model. Ignoring the $1/S$ corrections and weak temperature dependence of the bond parameters, we can take $g_x = f_y = g_{x+y} = S$, and obtain bare parameters of the sigma model $\chi_{\perp 0}^{-1} = 4(2J_2 + J_1)a^2$, $\rho_{x0} = (2J_2 + J_1)S^2$, and $\rho_{y0} = (2J_2 - J_1)S^2$. The spatial anisotropy is captured by two direction-dependent spin stiffness constants ρ_{x0} and ρ_{y0} , and $\chi_{\perp 0}$ is the bare uniform transverse susceptibility. The spin wave velocities before $1/S$ corrections are given by $v_{1x} = \sqrt{\rho_{x0}/\chi_{\perp 0}}$ and $v_{1y} = \sqrt{\rho_{y0}/\chi_{\perp 0}}$. The temperature dependence of the gap is determined by the bare Josephson energy scale

$$\Delta_{J0} = 2\pi\rho_0 = 4\pi J_2 S^2 \sqrt{1 - \frac{J_1^2}{4J_2^2}}, \quad (19)$$

where $\rho_0 = \sqrt{\rho_{x0}\rho_{y0}}$ is the bare, geometric mean stiffness constant. For parameter values $S = 1$ and $J_1/J_2 = 0.8$, we find $\Delta_{J0} = 11.5J_2$. After solving the mean-field equations, we obtain the Josephson energy scale

$$\Delta_J = \frac{\pi m v_{1y}}{a} = \pi m [(4J_2g_{x+y} + 2J_1g_x)(4J_2g_{x+y} - 2J_1f_y) + 2J_1f_y\mu]^{1/2}, \quad (20)$$

where m is the staggered magnetization at zero temperature and captures the $1/S$ corrections to Δ_J . For $S = 1$, $J_1/J_2 = 0.8$, we have found the zero-temperature parameters $m = 0.83$,

$g_x = 0.96$, $f_y = 0.91$, $g_{x+y} = 1.07$, and $\Delta_J = 10.54J_2$. Note that at $T = 0$, our calculation is consistent with that of Ref. 11. More details regarding the renormalized ρ and Δ_J obtained from a sigma model calculation will be discussed in Sec. V. Above $T_{\sigma 0}$, the nearest-neighbor bond correlations vanish, and two gaps become equal, $\Delta_1 = \Delta_2 = \sqrt{-\mu(8J_2g_{x+y} - \mu)}$. As the C_{4v} symmetry is restored above $T_{\sigma 0}$, the velocity anisotropy disappears and $v_{1x} = v_{1y} = v_{2x} = v_{2y} = 4J_2g_{x+y}a$.

IV. DYNAMIC STRUCTURE FACTOR

The dynamic structure factor is calculated in the modified spin wave theory through the average of the longitudinal and transverse spin structure factors. It is expressed as

$$\begin{aligned}
 \mathcal{S}(\mathbf{q}, \omega) &= \frac{1}{N} \sum_k \sum_{s, \bar{s}=\pm 1} [\cosh(2\theta_{\mathbf{k}+\mathbf{q}} - 2\theta_{\mathbf{k}}) - s\bar{s}] \\
 &\quad \times \delta(\omega - s\epsilon_{\mathbf{k}+\mathbf{q}} - \bar{s}\epsilon_{\mathbf{k}}) n_{\mathbf{k}+\mathbf{q}}^s n_{\mathbf{k}}^{\bar{s}}, \quad (21)
 \end{aligned}$$

where $n_{\mathbf{k}}^+ = n_{\mathbf{k}} + 1$ and $n_{\mathbf{k}}^- = n_{\mathbf{k}}$.

Consider first $\omega \ll T$, and low temperatures $T \ll \Delta_J$. The dominant contribution to $\mathcal{S}(\mathbf{q}, \omega)$ comes from the vicinity of the $(\pi, 0)$ wave vector. In the limit $|\pi - q_x| \ll \lambda_x^{-1} = T/v_x$ and $q_y \ll \lambda_y^{-1} = T/v_y$, we can analytically^{31,33,34} calculate $\mathcal{S}(\mathbf{q}, \omega)$, which satisfies a dynamic scaling relation

$$\mathcal{S}(\pi - q_x, q_y, \omega) = \tau \mathcal{S}_0(\pi - q_x, q_y) \Phi(z, \omega\tau), \quad (22)$$

where $\mathcal{S}_0(\pi - q_x, q_y)$ is the equal time structure factor, and $\tau = \Delta_J^{-1}$ is the scaling time. \mathcal{S}_0 also satisfies a scaling form $\mathcal{S}_0(\pi - q_x, q_y) = \xi_x \xi_y / (4\pi \lambda_y^2) \Lambda(z)$, where $z = [\xi_x^2(\pi - q_x)^2 + \xi_y^2 q_y^2]^{1/2} / 2$. The scaling functions are given by

$$\begin{aligned}
 \Phi(x, y) &= \frac{1}{2\Lambda(x)|y|\sqrt{x^2 + (x^2 - y^2)^2}} \left(\Theta(x^2 - y^2) \frac{2}{\pi} \right. \\
 &\quad \times \arctan \left[|y| \sqrt{\frac{x^2 - y^2}{x^2 + (x^2 - y^2)^2}} \right] \\
 &\quad \left. + \Theta(y^2 - x^2 - 1) \right), \\
 \Lambda(z) &= \frac{\log[z + \sqrt{1 + z^2}]}{z\sqrt{1 + z^2}}. \quad (23)
 \end{aligned}$$

When $z \rightarrow 0$, $\Lambda(z) \rightarrow 1$, and for $z \gg 1$, $\Lambda(z) \rightarrow \log(z)/z^2$. The second limit corresponds to momentum scales between inverse correlation length and inverse thermal length, where the system appears to have long-range order (Goldstone mode behavior). The results for \mathcal{S}_0 are in agreement with one loop scaling results of a quantum nonlinear sigma model.^{35,36}

A number of features follow from Eqs. (22) and (23). As a function of energy for a fixed \mathbf{q} with $z \gg 1$, $\mathcal{S}(\mathbf{q}, \omega)$ has a broad peak around $\omega \sim z/\tau$. As a function of \mathbf{q} for a fixed ω , $\mathcal{S}(\mathbf{q}, \omega)$ sharpens as temperature is reduced reflecting the increase of correlation length; this is also seen from the results of direct numerical calculations (Fig. 3). In the numerical calculations of $\mathcal{S}(\mathbf{q}, \omega)$ in Eq. (21), a Lorentzian broadening of the delta functions has been employed, and consequently the gap between $\omega\tau < z$ and $\omega\tau > \sqrt{z^2 + 1}$ is not observed in Fig. 3 but is instead left as shoulders. The processes beyond the

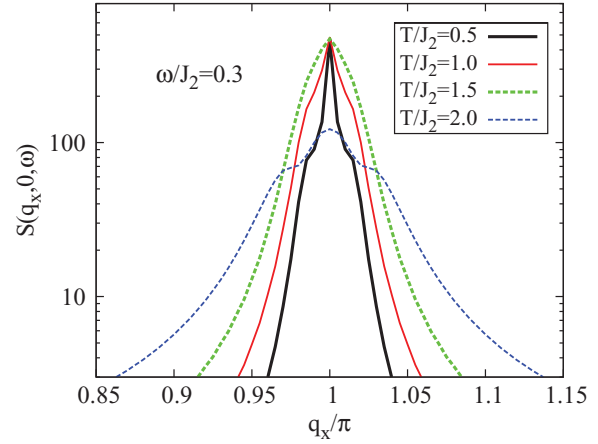


FIG. 3. (Color online) The sharpening of the dynamic structure factor around $(\pi, 0)$ with decreasing temperature for $\omega = 0.3J_2$, $S = 1$, and $J_1/J_2 = 0.8$.

modified spin wave theory are expected to smear the two-peak structure and also modify the scaling time τ to the phase coherence time $\sim (\Delta_J/T)^{1/2}/\Delta_1$.^{35,36}

Beyond the $\omega \ll T$ limit, we focus on the distribution of spectral weight in momentum space. Figures 4(a) and 4(b) illustrate the behavior at low energies. Provided $T < T_{\sigma 0}$, the anisotropy of the correlation lengths gives rise to an elliptic feature centered around $(\pi, 0)$. The overall size of the ellipses is reduced as the temperature is decreased, reflecting increasing correlation lengths. On the other hand, the ellipticity has only weak temperature dependence; the ratio of two correlation lengths is almost unaffected by temperature variations for $T \ll T_{\sigma 0}$, due to the weak temperature dependence of the velocity ratio v_{1x}/v_{1y} .

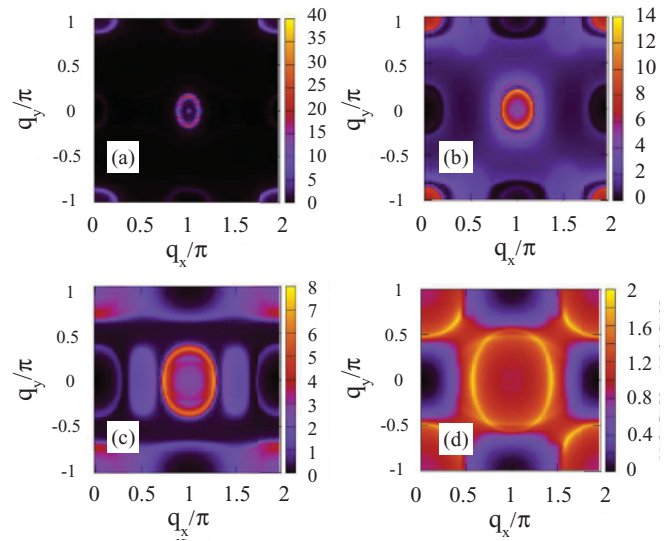


FIG. 4. (Color online) Distribution of the dynamic structure factor in the momentum space for different temperatures and energies. The temperatures and frequencies corresponding to panels (a)–(d) are respectively given by (a) $T/J_2 = 0.5$, $\omega/J_2 = 2.0$; (b) $T/J_2 = 2.1$, $\omega/J_2 = 2.0$; (c) $T/J_2 = 2.1$, $\omega/J_2 = 3.0$; (d) $T/J_2 = 2.1$, $\omega/J_2 = 4.5$.

With increasing energy, the evolution of the spectral weight distribution is illustrated in Figs. 4(b)–4(d). At intermediate energies, when ω is comparable to the peak energy in the dispersion $\epsilon_{\mathbf{k}}$ (see Fig. 2), there are features near $((1 \pm 1/2)\pi, 0)$, whose spectral weight is relatively small at the temperature shown in Fig. 4(c) but will increase with lowering temperature. The most visible spectral feature, however, is associated with the expanding ellipses surrounding $(\pm\pi, 0)$ and $(0, \pm\pi)$, as is clearly seen in the high-energy spectrum shown in Fig. 4(d).

V. THE ROLE OF ITINERANT ELECTRONS AND GINZBURG-LANDAU CONSIDERATIONS

A. Antiferromagnetic fluctuations

The description of the iron pnictides in terms of bad metals invokes quasilocalized moments coupled to itinerant electrons whose spectral weight depends on the proximity of the system to the Mott transition.⁹ For the parent compounds, the low-energy spin dynamics can be described in terms of a Ginzburg-Landau functional⁹ $\mathcal{S} = \mathcal{S}_2 + \mathcal{S}_4 + \dots$, where

$$\mathcal{S}_2 = \int d\mathbf{q} d\omega [r + wA_{\mathbf{Q}} + c\mathbf{q}^2 + \omega^2 + \gamma|\omega|](\mathbf{m}^2 + \mathbf{m}'^2) + v(q_x^2 - q_y^2)\mathbf{m} \cdot \mathbf{m}', \quad (24)$$

where \mathbf{m} and \mathbf{m}' are $O(3)$ vectors respectively for the magnetizations of the two decoupled sublattices, q_x and q_y are measured with respect to $(\pm\pi, 0)$ or $(0, \pm\pi)$, $w < 1$ is the coherent fraction of the single-electron spectral weight, and γ is the strength of spin damping caused by the coupling to the itinerant electrons. \mathcal{S}_4 contains not only terms of the form \mathbf{m}^4 , \mathbf{m}'^4 and $\mathbf{m}^2\mathbf{m}'^2$, but also an order-from-disorder term $(\mathbf{m} \cdot \mathbf{m}')^2$ with a negative coefficient.²⁸ Equation (24) implies that elliptic features will occur in the dynamical responses even in the regime where the Ising order is not static but fluctuating and short ranged; the primary role of the itinerant electrons, beyond shifting r through the positive $wA_{\mathbf{Q}}$ term, is to provide damping effects to such features.

Well below the mean-field Ising transition temperature, the thermal fluctuations of the Ising order parameter $\sigma = \pm(\mathbf{m} \cdot \mathbf{m}')/|\mathbf{m}||\mathbf{m}'|$ in the effective action of Eq. (24) can be ignored. The choice of $\sigma = \pm$ respectively correspond to short-range $(\pi, 0)$ or $(0, \pi)$ order. For short-range $(\pi, 0)$ order, $\mathbf{m} - \mathbf{m}'$ becomes gapped and we find that order parameter dynamics can be approximately determined in terms of a single $O(3)$ order parameter field $\mathbf{M} = \mathbf{m} + \mathbf{m}'$. The effective action for this field at quadratic order is given by

$$\mathcal{S}_2 \approx T \int d\mathbf{q} \sum_l [r + wA_{\mathbf{Q}} + q_x^2 v_x^2 + q_y^2 v_y^2 + \omega_l^2 + \gamma|\omega_l|] \mathbf{M}^2, \quad (25)$$

where $v_{x/y}^2 = (c \pm v/4)$, and $\omega_l = 2\pi Tl$ is the Matsubara frequency. With the further assumption of small-amplitude fluctuations, we can write $\mathbf{M} = M_0 \mathbf{n}$, where M_0 is the constant amplitude, and \mathbf{n} is the unit vector field. Thus low-energy dynamics is now determined by a damped, anisotropic nonlinear

sigma model. We consider the following damped nonlinear sigma model action:

$$\mathcal{S}_{\text{eff}} = \frac{T}{2vg} \int d^2q \sum_l [v^2 q^2 + \omega_l^2 + \gamma|\omega_l|] |\mathbf{n}(\mathbf{q}, \omega_l)|^2. \quad (26)$$

In writing the above equation we have rescaled $\sqrt{v_y/v_x} q_x \rightarrow q_x$, and $\sqrt{v_x/v_y} q_y \rightarrow q_y$, and $v = \sqrt{v_x v_y}$, to write the action in spatially isotropic form, and $g = v/\rho = v^{-1} \chi_{\perp}^{-1}$ is the coupling constant with dimension of length. The scaling behavior of the correlation length in the quantum disorder phase and quantum critical regime for this damped nonlinear sigma model has been analyzed in Ref. 44. Here we will only consider the thermally disordered or renormalized classical regime. In the large- N limit, the gap in the excitation spectrum Δ can be determined from the saddle-point equation

$$T \sum_l \int_{\bar{\Lambda}} \frac{d^2q}{(2\pi)^2} \frac{1}{v^2 q^2 + \omega_l^2 + \gamma|\omega_l| + \Delta^2} = \frac{1}{vg}, \quad (27)$$

where $\bar{\Lambda} \sim \pi/a$ is the momentum cutoff. The Matsubara sum can be performed in terms of digamma functions, and after the momentum integration the left-hand side can be expressed in terms of the logarithm of the gamma function. Here we consider two extreme limits of $\gamma/(2\pi T) \ll 1$ and $\gamma/(2\pi T) \gg 1$.

In the limit $\gamma/(2\pi T) \ll 1$, we obtain the $z = 1$ nonlinear sigma model result

$$\sinh \frac{\Delta}{2T} = \sinh \frac{v\bar{\Lambda}}{2T} \exp\left(\frac{2\pi v}{gT}\right). \quad (28)$$

In the limit of small temperatures, such that $v\bar{\Lambda} \gg T$, and $\Delta \ll T$, we obtain the result for the small γ limit,

$$\Delta = T \exp\left(-\frac{2\pi v}{T} \left(\frac{1}{g} - \frac{1}{g_{c1}}\right)\right) = T \exp\left(-\frac{2\pi\rho}{T}\right), \quad (29)$$

where $g_{c1} = 4\pi/\bar{\Lambda}$ is the coupling strength for the zero-temperature $z = 1$ quantum critical point, and ρ is the renormalized spin stiffness constant. From this expression we find $\xi = v/T \exp(\frac{2\pi\rho}{T})$ in the renormalized classical regime described by $T \ll 2\pi\rho$. For $2\pi\rho \gg T$, one obtains $z = 1$ quantum critical behavior $\xi \sim v/T$. If we go beyond the $N \rightarrow \infty$ limit, or perform a two loop renormalization group calculation in the renormalized classical regime, we will find the correct classical result $\xi \sim \exp(\frac{2\pi\rho}{T})$.^{34,35}

For $\gamma/(2\pi T) \gg 1$, the physical properties are governed by a $z = 2$ nonlinear sigma model. The frequency sum is performed after imposing a frequency cutoff $\omega_c = v^2 \bar{\Lambda}^2/\gamma$, and after performing the momentum integration we obtain

$$\frac{2\pi v}{gT} = \log \frac{v\bar{\Lambda}}{\Delta} + \log \Gamma\left(1 + \frac{2v^2 \bar{\Lambda}^2}{2\pi\gamma T} + \frac{\Delta^2}{2\pi\gamma T}\right) - 2 \log \Gamma\left(1 + \frac{v^2 \bar{\Lambda}^2}{2\pi\gamma T} + \frac{\Delta^2}{2\pi\gamma T}\right) + \log \Gamma\left(1 + \frac{\Delta^2}{2\pi\gamma T}\right). \quad (30)$$

Now in the limit $2v^2\bar{\Lambda}^2/(2\pi\gamma T) \gg 1$ and $\Delta^2/(2\pi\gamma T) \ll 1$, we can use the asymptotic behavior of the $\log \Gamma(1+x)$ to obtain the gap Δ at large Landau damping,

$$\Delta = v\bar{\Lambda} \exp\left(-\frac{2\pi v}{T}(1/g - 1/g_{c2})\right) = v\bar{\Lambda} \exp\left(-\frac{2\pi\rho}{T}\right), \quad (31)$$

with $1/g_{c2} = (v\bar{\Lambda}^2)(2\log 2 - 1)/(4\pi^2\gamma)$. Notice that correct renormalized classical behavior of the correlation length for large Landau damping is found from the saddle-point equation. For $2\pi\rho \ll T$ we find $z = 2$ quantum critical behavior $\Delta \sim \sqrt{2\pi\gamma T}$, augmented by logarithmic corrections. From the expressions of g_{c1} , g_{c2} we find that the stiffness for the $z = 2$ case is smaller than the $z = 1$ case. This reflects the role of Landau damping.

To summarize, in the limits of both small and large Landau damping, the correlation length has an exponential temperature dependence in the renormalized classical regime. This will be the basis of our fitting the correlation length, which is described in Appendix A.

If we consider the effects of the interlayer antiferromagnetic exchange coupling J_z in addition to the $J_1 - J_2$ model by using modified spin wave theory (see Appendix C), we obtain a finite mean-field antiferromagnetic transition temperature T_{N0} . Within the Ginzburg-Landau framework this corresponds to setting $r(T) = 0$. The fermion contribution $wA_{\mathbf{Q}}$ being positive will decrease the transition temperature from the mean-field value T_{N0} to a smaller value T_N . However there will be a significant amount of three-dimensional antiferromagnetic fluctuations up to the mean-field Néel temperature T_{N0} . Above T_{N0} the magnetic fluctuations are essentially two dimensional.

B. Ising fluctuations

Since the Ising order parameter breaks C_{4v} symmetry, and in particular corresponds to B_{1g} representation of the tetragonal lattice, it will couple to all the singlet fermion bilinears, which correspond to B_{1g} representation. Without the loss of generality if we consider a two-orbital model of fermions including only d_{xz} and d_{yz} orbitals, the Ising order parameter σ will couple to $(\cos k_x - \cos k_y)\Psi_{\mathbf{k}_s}^\dagger \Psi_{\mathbf{k}_s}$, $\Psi_{\mathbf{k}_s}^\dagger \tau_3 \Psi_{\mathbf{k}_s}$, $(\cos k_x + \cos k_y)\Psi_{\mathbf{k}_s}^\dagger \tau_3 \Psi_{\mathbf{k}_s}$, and $\cos k_x \cos k_y \Psi_{\mathbf{k}_s}^\dagger \tau_3 \Psi_{\mathbf{k}_s}$, etc., where $\Psi_{\mathbf{k}_s}^\dagger = (c_{xz, \mathbf{k}_s}^\dagger, c_{yz, \mathbf{k}_s}^\dagger)$ describes the orbital and spin dependent fermion creation operators and the Pauli matrix τ_3 acts on the orbital basis. Among the various B_{1g} bilinears, the conventional nematic order parameter and the ferro-orbital order parameter respectively correspond to $(\cos k_x - \cos k_y)\Psi_{\mathbf{k}_s}^\dagger \Psi_{\mathbf{k}_s}$ and $\Psi_{\mathbf{k}_s}^\dagger \tau_3 \Psi_{\mathbf{k}_s}$. Notice that we can couple other d orbitals, following the same symmetry-based criterion. When we integrate out the itinerant fermions, the contributions to the Ising order parameter σ will arise from generalized B_{1g} particle-hole susceptibilities, and the quadratic part of the low-energy action for σ will have the form

$$S_2[\sigma] = \int d\mathbf{q} \sum_l \left[r_\sigma + wA_0 + q^2 + \gamma_\sigma \frac{|\omega_l|}{q} \right] |\sigma(\mathbf{q}, \omega_l)|^2. \quad (32)$$

In the above equation γ_σ is the Landau damping strength, and r_σ is the mass term arising from the localized model, and $wA_0 > 0$ is the fermion contribution to the Ising mass. This fermionic contribution will suppress the Ising transition temperature from its mean-field value $T_{\sigma 0}$ to T_σ . But, the correlation length of the Ising order parameter will remain appreciable up to the mean-field temperature $T_{\sigma 0}$. Since the Ising transition occurs due to in-plane magnetic fluctuations, consideration of interlayer coupling does not significantly modify the Ising correlations.

When we consider the magnetic and Ising order parameter fluctuations on the same footing, further changes in the transition temperatures will arise from the self-interaction of σ , \mathbf{m} , \mathbf{m}' , and their mutual interaction $\sigma \mathbf{m} \cdot \mathbf{m}'$. The interplay of Ising and magnetic order parameters and their self-interactions are crucial to determining whether there will be a concomitant first-order transition or two separate second-order phase transitions. Despite the suppression of actual transition temperatures and the possible complexity regarding the actual nature of the transitions, we still expect that the correlation lengths of the magnetic and the Ising order parameters will remain sizable up to their respective mean-field transition temperatures.

VI. IMPLICATIONS FOR IRON PNICTIDES

Our detailed theoretical studies provide the basis to understand the anisotropic spin responses that have been observed in the paramagnetic phase of the parent iron pnictides CaFe_2As_2 .²⁷ These observations, made at temperatures above the first-order antiferromagnetic/structural transition, can be understood if the transition temperature is assumed to be considerably lower than the mean-field Ising transition temperature by the effects of fluctuations and coupling to phonons. To compare our theoretical results with the experiments of Ref. 27 we have fitted the low-frequency experimental data with the dynamic structure factor calculated within the saddle-point approximation of an anisotropic, damped nonlinear sigma model, which follows from the action of Eq. (24). Within the saddle-point approximation the imaginary part of the staggered susceptibility is given by

$$\chi''(\mathbf{q} - \mathbf{Q}, \omega) = \frac{\chi_\perp^{-1} \gamma \omega}{\gamma^2 \omega^2 + [\omega^2 - v_x^2(q_x - \pi)^2 - v_y^2 q_y^2 - \Delta^2]^2}. \quad (33)$$

The velocities of the effective model are taken from the modified spin wave calculations. The details of our procedure are provided in Appendix A.

The comparison of our results with those of Ref. 27 is shown in Fig. 5. The calculated elliptic features of $\mathcal{S}(\mathbf{q} - \mathbf{Q}, \omega)$ [Fig. 5(a)] is compatible with that seen experimentally [Fig. 5(b)] at low frequencies. This continues to be the case at higher frequencies, as shown in Figs. 5(c) and 5(d). The experimental results in the paramagnetic phase are consistent with our conclusions that as temperature is lowered, the peaks in the momentum space sharpen but the ellipticity is only weakly affected. Our estimated values of exchange constants are consistent with those of Ref. 27. When ω is smaller than the excitation gap Δ , the dynamic structure factor is peaked at

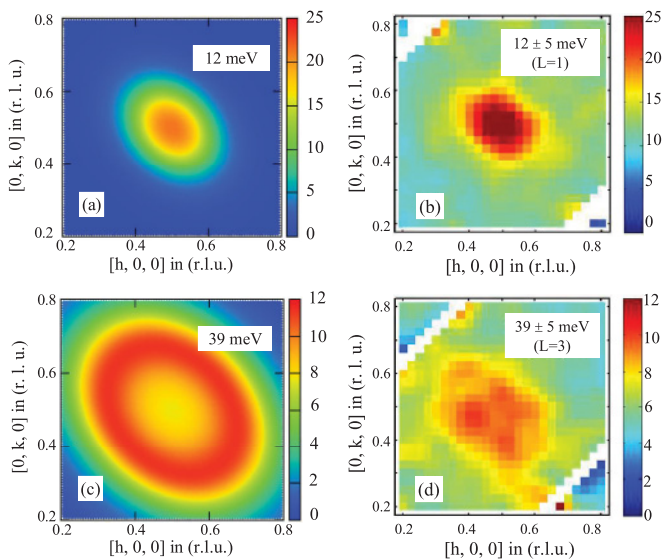


FIG. 5. (Color online) Panels (a) and (b) respectively demonstrate $\mathcal{S}(\mathbf{q} - \mathbf{Q}, \omega = 12 \text{ meV})$ at $T = 180 \text{ K}$ obtained from our theory and data of Ref. 27. Panels (c) and (d) respectively demonstrate $\mathcal{S}(\mathbf{q} - \mathbf{Q}, \omega = 39 \text{ meV})$ at $T = 180 \text{ K}$ obtained from our theory and data of Ref. 27. We have used $J_1/J_2 = 0.55$ (Ref. 27), $J_2 = 9.8 \text{ meV}$, and $\gamma = 47 \text{ meV}$. To facilitate the comparison with experimental result, we have plotted here in the Brillouin zone corresponding to the two-Fe unit cell instead of that for the one-Fe unit cell used in the rest of the paper.

$\mathbf{q} = \mathbf{Q}$. For $\omega > \Delta$, the intensity peak gets shifted to $|\mathbf{q} - \mathbf{Q}| = \sqrt{\omega^2 - \Delta^2}/v$ as shown in Fig. 5(c), and the ω^2 term in the dynamics is important to capture this feature also observed in the experiment as shown in Fig. 5(d).

Interlayer magnetic couplings in the parent iron arsenides vary considerably among the materials, but are always relatively weak. In Ref. 27, the interlayer coupling J_z in paramagnetic CaFe_2As_2 was shown to be very weak, with $J_z/J_2 = 0.1$, being smaller than its counterpart in the magnetically ordered phase at low temperature. Consideration of such a weak interlayer coupling does not appreciably change the estimated exchange constants and the in-plane spin dynamics. An estimation of the spin stiffness constant using a renormalized classical approximation for the correlation length shows that both fermion-induced moment reduction and Landau damping can sufficiently renormalize the stiffness constant (see Appendix A). In Appendix B we have considered the effects of the weak interlayer exchange coupling J_z using the modified spin wave theory. For $J_z/J_2 = 0.1$ the mean-field Néel temperature T_{N0} and the mean-field Ising transition temperature $T_{\sigma 0}$ become very close. However as we have discussed in Sec. V, despite the suppression of the actual transition temperature due to various fluctuation mechanisms, the magnetic and the Ising correlation lengths remain sizable up to the mean-field transition temperatures. In the temperature regime $T_N < T < T_{N0}$, there are three-dimensional antiferromagnetic fluctuations. However if we consider the ratio of the in-plane and interplane correlation lengths (measured in units of corresponding lattice spacing), we find $\xi_z/\xi_x \approx [J_z/(2J_2 + J_1)]^{1/2}$. This ratio is of course material dependent. For weak inter-layer coupling of Ref. 27, this ratio is

~ 0.2 , and magnetic fluctuations are indeed quasi-two-dimensional.

Finally our discussion regarding the effect of itinerant electrons is most pertinent to the parent systems, but is consistent with the experimental observation of similar low-energy anisotropic responses in the carrier-doped iron pnictides.^{37–39}

VII. SUMMARY AND CONCLUSIONS

We have addressed the spin dynamics in the paramagnetic phase of a two-dimensional $J_1 - J_2$ antiferromagnet on a square lattice at a finite temperature, using modified spin wave theory. Within the modified spin wave theory we have identified a mean-field Ising transition temperature $T_{\sigma 0}$, below which the C_{4v} symmetry of the square lattice is spontaneously broken. In the Ising ordered phase the system demonstrates short-range $(\pi, 0)$ or $(0, \pi)$ antiferromagnetic order. In order to systematically understand the finite-temperature spin dynamics in the paramagnetic phase of iron pnictides, we have described the fermionic contributions and self-interaction effects of the order parameter fields within a Ginzburg-Landau framework. We have found that the fermion contribution and the self-interaction effects can considerably decrease the Néel and the Ising transition temperatures from their corresponding mean-field values. However the correlation lengths of the magnetic and Ising order parameters can remain appreciable up to the mean-field transition temperatures. Based on this assumption, we have fitted the experimental data of Ref. 27, using our theoretical results. The calculated anisotropic features of the spin response are compatible with experiments for different frequencies.

Finally, our calculations of the spin fluctuations at high energies should help understand future experiments. The high-energy spin spectrum at the low-temperature ordered state of CaFe_2As_2 (Ref. 23) has already provided valuable information on the x - y anisotropy of the exchange interactions. Similar experiments have recently been reported in BaFe_2As_2 (Ref. 40) and SrFe_2As_2 (Ref. 41), including at temperatures just above the Néel transition where strong orbital anisotropy has developed.^{42,43} It will be instructive to experimentally map out the high-energy spectrum at higher temperatures in the paramagnetic phase.

ACKNOWLEDGMENTS

We thank S. Chakravarty, P. Dai, R. J. McQueeney, and A. Nevidomskyy for valuable discussions, and NSF Grant No. DMR-1006985, the Robert A. Welch Foundation Grant No. C-1411, and the W. M. Keck Foundation for support.

APPENDIX A: PROCEDURE FOR COMPARING WITH THE EXPERIMENTAL DATA

We analyze the experimental data of Ref. 27 by using the imaginary part of the staggered susceptibility $\chi(\mathbf{q} - \mathbf{Q}, \omega)$,

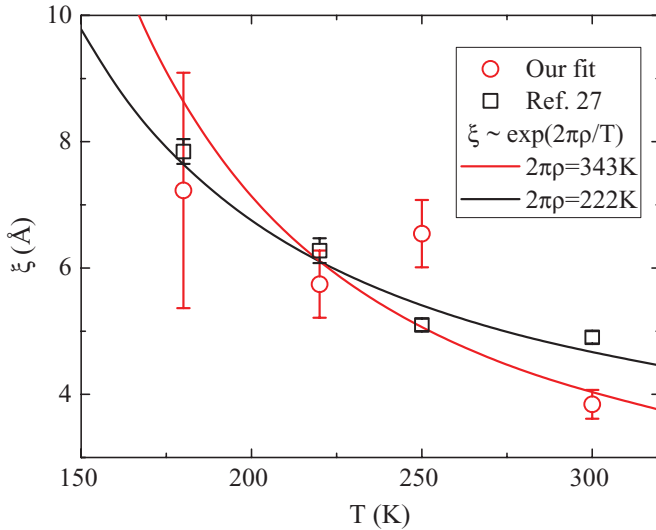


FIG. 6. (Color online) Comparison between the correlation lengths $\xi = \sqrt{\xi_x \xi_y}$ extracted from our fitting and that of Ref. 27. The fitted spin stiffness constants are shown in the inset.

which is calculated within the saddle-point approximation for Eq. (26). From the saddle-point calculation we find

$$\chi''(\mathbf{q} - \mathbf{Q}, \omega) = \frac{\chi_{\perp}^{-1} \gamma \omega}{\gamma^2 \omega^2 + [\omega^2 - v_x^2 (q_x - \pi)^2 - v_y^2 q_y^2 - \Delta^2]^2}. \quad (\text{A1})$$

At $\mathbf{q} = \mathbf{Q}$, we have

$$\chi''(0, \omega) = \frac{\chi_{\perp}^{-1} \gamma \omega}{\gamma^2 \omega^2 + (\omega^2 - \Delta^2)^2}, \quad (\text{A2})$$

where χ_{\perp} is the uniform transverse susceptibility. We calculate the velocities v_x and v_y using Eq. (13) and Eq. (14), and for the exchange constants we choose $J_2 = 10$ meV and $J_1 = 0.55 J_2 = 5.5$ meV, as determined by Diallo *et al.*²⁷ By fitting the experimental data we determine the temperature-independent Landau damping strength γ and the temperature-dependent gap Δ . By fitting the data for $\chi''(0, \omega)$ at $T = 180$ K with the formula from Eq. (A2), we find the Landau damping strength γ and the gap Δ at 180 K. At low frequencies, Eq. (A2) can be further approximated by a Lorentzian with a width $\Gamma_T \approx \Delta^2 / \sqrt{\gamma^2 - 2\Delta^2}$. At the relatively low temperature of 180 K, the Lorentzian form is a good fit to Eq. (A2) up to frequencies of about 40 meV, and $\Gamma_T = 7$ meV. At the high temperature of 300 K, the Lorentzian form, which becomes a poorer fit to Eq. (A2) over the same frequency range, yields $\Gamma_T = 44$ meV. The definition of the energy linewidth as Γ_T is the same notation as used in Ref. 27, but the constant

γ used in Ref. 27 is not the conventional Landau damping strength and has a different meaning from ours. Our estimation is $\gamma = 47$ meV. For the available data at nonzero $\mathbf{q} - \mathbf{Q}$ at different temperatures, we use the value of γ so determined, and find the Δ at different temperatures. Using the values of v_x , v_y , and Δ , we find the correlation length ξ_x and ξ_y . The comparison of our theoretically calculated dynamic structure factor with the fitted parameter values, and the experimental results at low frequency 12 meV, is shown in Fig. 5(a) and Fig. 5(b). Even at higher energy $\omega = 39$ meV our results for the dynamic structure factor are in reasonable agreement with experimental data, and the comparison for this frequency is shown in Fig. 5(c) and Fig. 5(d). The consideration of the ω^2 term in the effective action leads to an interesting feature of the dynamic structure factor. For low frequencies such that $\omega < \Delta$, $\chi''(\mathbf{q} - \mathbf{Q}, \omega)$ is peaked at $\mathbf{q} = \mathbf{Q}$. But at higher frequencies such that $\omega > \Delta$, the intensity peak occurs away from the antiferromagnetic wave vector and its location is determined by $|\mathbf{q} - \mathbf{Q}| = \sqrt{\omega^2 - \Delta^2}/v$. This shift in the intensity peak can clearly be seen by comparing Fig. 5(a) and Fig. 5(c). Similar shift in the intensity peak can also be seen in the experimental results by comparing Fig. 5(b) and Fig. 5(d). For the correlation length we have compared our and experimental results in Fig. 6 by plotting the temperature dependence of the geometric mean of ξ_x and ξ_y . By fitting the correlation length with the renormalized classical formula, we have obtained an estimation for the stiffness constant. The fermion-induced reduction of the magnetic moment M_0 and Landau damping are found to significantly reduce the stiffness constant in comparison to a pure $J_1 - J_2$ model.

APPENDIX B: EFFECTS OF INTERLAYER EXCHANGE COUPLING

The quasi-2D nature of the spin dynamics was clearly shown in Ref. 27. To explain the observed $(\pi, 0, \pi)$ antiferromagnetic order, an interlayer antiferromagnetic coupling J_z was assumed and J_z was estimated to be $\sim 0.1 J_2$. To assess the effects of J_z on the spin dynamics we first incorporate the three-dimensional effects in our modified spin wave theory calculations. For simplicity we assume the sublattice angle $\phi = \pi$. The modification to our discussion in Sec. I comes through an additional interlayer antiferromagnetic bond correlation parameter g_z . The Ising transition will be determined by the vanishing of in-plane nearest neighbor bond correlations g_x and f_y . In the presence of J_z , there is a finite, mean-field antiferromagnetic transition temperature T_{N0} , corresponding to Bose condensation of a 's. The expression for total energy in Eq. (5) changes into

$$E = -\frac{J_1 N}{2} \sum_{\delta_1 = \pm \hat{x}} \left(S + \frac{1}{2} - f(0) + g_x \right)^2 + \frac{J_1 N}{2} \sum_{\delta_2 = \pm \hat{y}} \left(S + \frac{1}{2} - f(0) + f_y \right)^2 - \frac{J_2 N}{2} \sum_{\delta_3 = \pm \hat{x} \pm \hat{y}} \left(S + \frac{1}{2} - f(0) + g_{x+y} \right)^2 - \frac{J_z N}{2} \sum_{\delta_1 = \pm \hat{z}} \left(S + \frac{1}{2} - f(0) + g_x \right)^2, \quad (\text{B1})$$

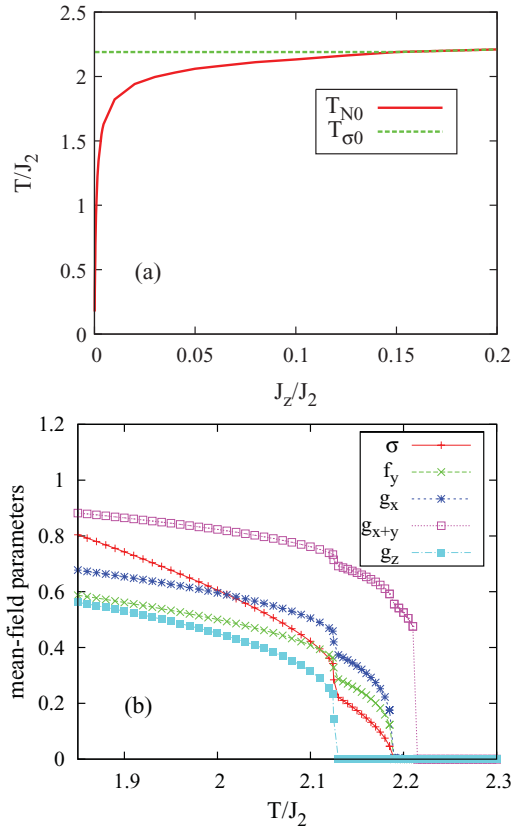


FIG. 7. (Color online) Panel (a) shows the comparison between the mean-field Néel temperature T_{N0} and mean-field Ising transition temperature $T_{\sigma 0}$, as a function of the interplanar coupling J_z , for $J_1/J_2 = 0.8$ and $S = 1$. Panel (b) shows the temperature dependence of different mean-field parameters for $J_z/J_2 = 0.1$.

and the expressions for $A_{\mathbf{k}}$ and $B_{\mathbf{k}}$ are modified according to

$$A_{\mathbf{k}} = 2J_1 g_x C_{x,\mathbf{k}} + 4J_2 g_{x+y} C_{x+y,\mathbf{k}} + 2J_z g_z C_{z,\mathbf{k}}, \quad (\text{B2})$$

$$B_{\mathbf{k}} = 2J_1 (g_x - f_y) + 2J_1 f_y C_{y,\mathbf{k}} + 4J_2 g_{x+y} - \mu + 2J_z g_z, \quad (\text{B3})$$

where $C_{z,\mathbf{k}} = \cos k_z c$, and c is the interlayer separation. After accounting for the possibility of a finite staggered magnetization below T_{N0} , the mean-field equations are given by

$$f_y = m_0 + \frac{1}{N} \sum_{\mathbf{k}} \frac{B_{\mathbf{k}}}{\epsilon_{\mathbf{k}}} \left(n_{\mathbf{k}} + \frac{1}{2} \right) C_{y,\mathbf{k}}; \quad (\text{B4})$$

$$g_{\alpha} = m_0 + \frac{1}{N} \sum_{\mathbf{k}} \frac{A_{\mathbf{k}}}{\epsilon_{\mathbf{k}}} \left(n_{\mathbf{k}} + \frac{1}{2} \right) C_{\alpha,\mathbf{k}}, \quad \alpha = x, x+y, z; \quad (\text{B5})$$

$$S + \frac{1}{2} = m_0 + \frac{1}{N} \sum_{\mathbf{k}} \frac{B_{\mathbf{k}}}{\epsilon_{\mathbf{k}}} \left(n_{\mathbf{k}} + \frac{1}{2} \right). \quad (\text{B6})$$

For $S = 1$, $J_1/J_2 = 0.8$, $c = a$, the dependence of T_{N0} and $T_{\sigma 0}$ on J_z/J_2 are shown in Fig. 7(a). The temperature dependence of the mean-field bond parameters for $J_z/J_2 = 0.1$ are shown in Fig. 7(b). With increasing J_z , the Néel temperature gradually increases and asymptotically approaches $T_{\sigma 0}$. Since the mean-field Ising transition is a consequence of the two-dimensional magnetic fluctuations, $T_{\sigma 0}$ is not modified by the finite interlayer coupling J_z . For $J_z/J_2 = 0.1$ and $J_2 \sim 10$ meV we obtain $T_{N0} \approx T_{\sigma 0} \sim 240$ K, which is much higher than the actual Néel and structural transition temperature. Therefore the fluctuating anisotropy effects will be important over a wide range of temperature, and the finite J_z does not change this conclusion.

Below $T_{\sigma 0}$, by expanding the dispersion around $\mathbf{Q} = (\pi, 0, \pi)$, we obtain

$$\epsilon_{\mathbf{k}} = [v_x^2(\pi - k_x)^2 + v_y^2 k_y^2 + v_z^2(\pi - k_z)^2 + \Delta^2]^{1/2}, \quad (\text{B7})$$

$$\Delta = [-\mu(8J_2 g_{x+y} + 4J_1 g_x + 4J_z g_z - \mu)]^{1/2}, \quad (\text{B8})$$

$$\mu = 0, \text{ for } T < T_N, \quad (\text{B8})$$

$$v_x = a[(4J_2 g_{x+y} + 2J_1 g_x)(4J_2 g_{x+y} + 2J_1 g_x + 2J_z g_z)]^{1/2}, \quad (\text{B9})$$

$$v_y = a[(4J_2 g_{x+y} + 2J_1 g_x + 2J_z g_z)(4J_2 g_{x+y} - 2J_1 f_y + 2J_1 f_y \mu)]^{1/2}, \quad (\text{B10})$$

$$v_z = c[(4J_2 g_{x+y} + 2J_1 g_x + 2J_z g_z)2J_z g_z]^{1/2}. \quad (\text{B11})$$

We further notice that the velocities are well approximated by

$$v_x \approx 2Sa(J_1 + 2J_2) \sqrt{1 + \frac{J_z}{J_1 + 2J_2}}, \quad (\text{B12})$$

$$v_y \approx v_x \sqrt{\frac{2J_2 - J_1}{2J_2 + J_1}}, \quad (\text{B13})$$

$$v_z \approx v_x \frac{c}{a} \sqrt{\frac{J_z}{2J_2 + J_1}}, \quad (\text{B14})$$

and even in the presence of finite J_z , the ratio v_y/v_x remains unchanged. For $J_z/J_2 = 0.1$ and $c/a \approx 3.026$,²⁷ we obtain $v_z/v_x \sim 0.6$, and this leads to smaller interplanar correlation length ($\xi_z < \xi_x, \sqrt{\xi_x \xi_y}$). In our comparison with experiments we have looked at the data that correspond to in-plane dynamics, i.e., $\mathbf{q} - \mathbf{Q} = (q_x - \pi, q_y, 0)$, and consequently all the formulas remain unaffected. We also note that the effects of interplanar coupling inside the magnetically ordered phase have been considered in Refs. 45–47 using similar techniques. However our results are derived for the paramagnetic phase and are essentially different from those described in Refs. 45–47.

¹Y. Kamihara, T. Watanabe, M. Hirano, and H. Hosono, *J. Am. Chem. Soc.* **130**, 3296 (2008).

²Z. A. Ren *et al.*, *Chin. Phys. Lett.* **25**, 2215 (2008).

³C. de la Cruz *et al.*, *Nature (London)* **453**, 899 (2008).

⁴Q. Si and E. Abrahams, *Phys. Rev. Lett.* **101**, 076401 (2008).

⁵T. Yildirim, *Phys. Rev. Lett.* **101**, 057010 (2008).

⁶F. Ma, Z-Y. Lu, and T. Xiang, *Phys. Rev. B* **78**, 224517 (2008).

⁷C. Fang, H. Yao, W. F. Tsai, J. P. Hu, and S. A. Kivelson, *Phys. Rev. B* **77**, 224509 (2008).

- ⁸C. Xu, M. Muller, and S. Sachdev, *Phys. Rev. B* **78**, 020501(R) (2008).
- ⁹Q. Si, E. Abrahams, J. Dai, and J.-X. Zhu, *New J. Phys.* **11**, 045001 (2009).
- ¹⁰J. Dai, Q. Si, J. X. Zhu, and E. Abrahams, *Proc. Natl. Acad. Sci. USA* **106**, 4118 (2009).
- ¹¹G. S. Uhrig, M. Holt, J. Oitmaa, O. P. Sushkov, and R. R. P. Singh, *Phys. Rev. B* **79**, 092416 (2009).
- ¹²S. Graser, T. A. Maier, P. J. Hirschfeld, and D. J. Scalapino, *New J. Phys.* **11**, 025016 (2009).
- ¹³Y. Ran, F. Wang, H. Zhai, A. Vishwanath, and D. H. Lee, *Phys. Rev. B* **79**, 014505 (2009).
- ¹⁴J. Knolle, I. Eremin, A. V. Chubukov, and R. Moessner, *Phys. Rev. B* **81**, 140506(R) (2010).
- ¹⁵M. Qazilbash *et al.*, *Nature Phys.* **5**, 647 (2009).
- ¹⁶W. Z. Hu *et al.*, *Phys. Rev. Lett.* **101**, 257005 (2008).
- ¹⁷J. Yang *et al.*, *Phys. Rev. Lett.* **102**, 187003 (2009).
- ¹⁸A. V. Boris *et al.*, *Phys. Rev. Lett.* **102**, 027001 (2009).
- ¹⁹K. Haule, J. H. Shim, and G. Kotliar, *Phys. Rev. Lett.* **100**, 226402 (2008).
- ²⁰A. Kutepov, K. Haule, S. Y. Savrasov, and G. Kotliar, *Phys. Rev. B* **82**, 045105 (2010).
- ²¹J. X. Zhu *et al.*, *Phys. Rev. Lett.* **104**, 216405 (2010).
- ²²M. Fang *et al.*, *Europhys. Lett.* **94**, 27009 (2011).
- ²³J. Zhao *et al.*, *Nature Phys.* **5**, 555 (2009).
- ²⁴R. R. P. Singh, e-print arXiv:0903.4408v1 (2009).
- ²⁵F. Krüger, S. Kumar, J. Zaanen, and J. van den Brink, *Phys. Rev. B* **79**, 054504 (2009).
- ²⁶W. Lv, F. Krüger, and P. Phillips, *Phys. Rev. B* **82**, 045125 (2010).
- ²⁷S. O. Diallo *et al.*, *Phys. Rev. B* **81**, 214407 (2010).
- ²⁸P. Chandra, P. Coleman, and A. I. Larkin, *Phys. Rev. Lett.* **64**, 88 (1990).
- ²⁹R. Flint and P. Coleman, *Phys. Rev. B* **79**, 014424 (2009).
- ³⁰M. Takahashi, *Phys. Rev. B* **40**, 2494 (1989).
- ³¹A. Auerbach and D. P. Arovas, *Phys. Rev. Lett.* **61**, 617 (1988).
- ³²H. Nishimori and Y. Saika, *J. Phys. Soc. Jpn.* **59**, 4454 (1990).
- ³³P. Kopietz, *Phys. Rev. Lett.* **64**, 2587 (1990).
- ³⁴M. Takahashi, *Prog. Theor. Phys.* **101**, 487 (1990).
- ³⁵S. Chakravarty, B. I. Halperin, and D. R. Nelson, *Phys. Rev. B* **39**, 2344 (1989).
- ³⁶A. V. Chubukov, S. Sachdev, and J. Ye, *Phys. Rev. B* **49**, 11919 (1994).
- ³⁷C. Lester *et al.*, *Phys. Rev. B* **81**, 064505 (2010).
- ³⁸H.-F. Li *et al.*, *Phys. Rev. B* **82**, 140503(R) (2010).
- ³⁹J. T. Park *et al.*, *Phys. Rev. B* **82**, 134503 (2010).
- ⁴⁰L. W. Harriger *et al.*, *Phys. Rev. B* **84**, 054544 (2011).
- ⁴¹R. A. Ewings *et al.*, *Phys. Rev. B* **83**, 214519 (2011).
- ⁴²M. Yi *et al.*, *Proc. Natl. Acad. Sci. USA* **108**, 6878 (2011).
- ⁴³J. H. Chu *et al.*, *Science* **329**, 824 (2010).
- ⁴⁴S. Sachdev, A. V. Chubukov, and A. Sokol, *Phys. Rev. B* **51**, 14874 (1995).
- ⁴⁵A. Smerald and N. Shannon, *Europhys. Lett.* **92**, 47005 (2010).
- ⁴⁶M. Holt, O. P. Sushkov, D. Stanek, and G. S. Uhrig, *Phys. Rev. B* **83**, 144528 (2011).
- ⁴⁷A. Ong, G. S. Uhrig, and O. P. Sushkov, *Phys. Rev. B* **80**, 014514 (2009).